Protective effects of PDGF-AB/BB against cellular senescence in human intervertebral disc

Changli Zhang[1, 2], Martha Elena Diaz-Hernandez[1, 2], Takanori Fukunaga[1, 2], Shenoy Sreekala[1,2], Sangwook Tim Yoon[3], Lisbet Haglund[4], Hicham Drissi[1, 2]

[1]Department of Orthopaedics, Emory University School of Medicine, Atlanta, GA, USA

[2]Atlanta VA Medical Center, Decatur, GA, USA

[3]Emory Orthopaedics & Spine Center, Atlanta, GA, USA

[4]Department of Surgery, McGill University, Montreal, Qc., Canada

Corresponding author:

Hicham Drissi, PhD

hicham.drissi@emory.edu

Key words: PDGF, cellular senescence, intervertebral disc degeneration, irradiation, oxidative stress, reactive oxygen species.

Abstract

Cellular senescence, characterized by a permanent state of cell cycle arrest and a secretory phenotype contributing to inflammation and tissue deterioration, has emerged as a target for age-related interventions. Accumulation of senescent cells is closely linked with intervertebral disc (IVD) degeneration, a prevalent age-dependent chronic disorder causing low back pain. Previous studies have highlighted that platelet-derived growth factor (PDGF) mitigated IVD degeneration through anti-apoptosis, anti-inflammation, and pro-anabolism. However, its impact on IVD cell senescence remains elusive. In this study, human NP and AF cells derived from aged, degenerated IVDs were treated with recombinant human (rh) PDGF-AB/BB for 5 days and changes of transcriptome profiling were examined through mRNA sequencing. NP and AF cells demonstrated similar but distinct responses to the treatment. However, the effects of PDGF-AB and BB on human IVD cells were comparable. Specifically, PDGF-AB/BB treatment resulted in downregulation of gene clusters related to neurogenesis and response to mechanical stimulus in AF cells while the downregulated genes in NP cells were mainly associated with metabolic pathways. In both NP and AF cells, PDGF-AB and BB treatment upregulated the expression of genes involved in cell cycle regulation, mesenchymal cell differentiation, and response to reduced oxygen levels, while downregulating the expression of genes related to senescence associated phenotype, including oxidative stress, reactive oxygen species (ROS), and mitochondria dysfunction. Network analysis revealed that PDGFRA and IL6 were the top hub genes in treated NP cells. Furthermore, in irradiation-induced senescent NP cells, PDGFRA gene expression was significantly reduced compared to non-irradiated cells. However, rhPDGF-AB/BB treatment increased PDGFRA expression and mitigated the senescence progression through increased cell population in the S phase, reduced SA-β-Gal activity, and decreased expression of senescence related regulators including P21, P16, IL6, and NF-κB. Our findings reveal a novel anti-senescence role of PDGF in the IVD, demonstrating its ability to alleviate the senescent phenotype and protect against the progression of senescence. This makes it a promising candidate for preventing or treating IVD degeneration by targeting cellular senescence.

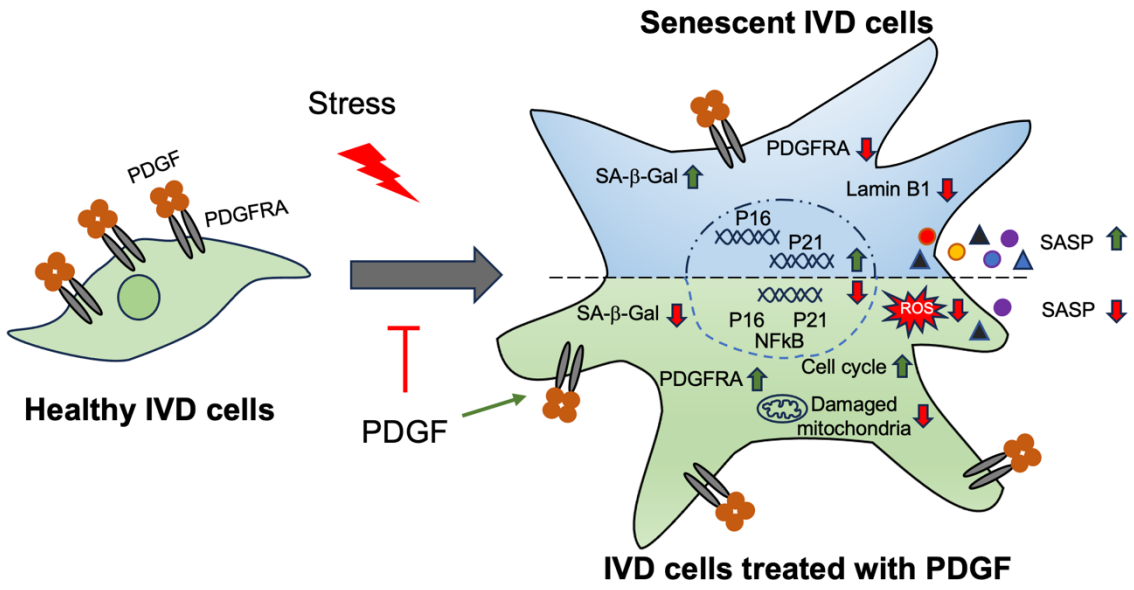

Introduction

Low back pain (LBP), ranked as the first cause of years lived with disability, is a prevalent condition. Although the etiology of LBP is multifactorial, a major contributor of LBP is intervertebral disc (IVD) degeneration, which is increasing exponentially due to a growing aged population worldwide (1). Current treatments, such as medicine, physical therapy, and surgical excision of the herniated tissues, only temporally alleviate painful symptoms (2). In fact, patients often experience persistent LBP after surgery (3). The fundamental cause of this is the inadequate knowledge of the underlying pathophysiology mechanisms leading to IVD degeneration. Therefore, it is crucial to understand the pathogenesis of IVD degeneration and develop novel therapeutic interventions to mitigate the degenerative processes.

The IVD consists of three compartments: the gelatinous nucleus pulposus (NP), fibrous annulus fibrosus (AF), and cartilaginous endplate (4). NP and AF tissues play distinct yet complementary roles in maintaining the spinal function. The NP has high content of proteoglycans and water, absorbing and distributing mechanical forces. In contrast, AF consists of multiple layers of concentric lamellae, which provides strength and stability to the disc and withstands compressive forces (4,5). To date, the main focus of IVD cell studies has been on the NP. It is often the first site impacted during aging and degeneration, indicating the crucial role of NP cells in the initiation of IVD degeneration. In contrast, degenerated alterations in the AF are more closely linked to pain and disability. As a result, effective therapeutic strategies for IVD degeneration should aim to restore the functionality of the entire disc unit.

Cellular senescence, triggered by normal cells in response to various intrinsic and extrinsic stressors, is a fundamental mechanism underlying age-related chronic diseases. Senescent cells are featured by irreversible growth arrest and acquire a senescent-associated secretory phenotype (SASP) and the secretion of pro-inflammatory cytokines, chemokines, and tissue-damaging proteases (6). Activation of P53/P21 and P16 pathways play a critical role in regulating senescence (7). In addition, NF-κB pathway is a major pathway involved in the expression of pro-inflammatory mediators in senescent cells (8). Factors within the SASP can act in an autocrine manner to reinforce the senescent state and induce senescence in neighboring cells via paracrine signaling (9). This mechanism elucidates the accumulation of senescent cells with aging and its associated detrimental effects. In the IVD, it has been well established that the number of senescent cells increases with aging and IVD

degeneration (10–12), as demonstrated by increased senescence-associated β-galactosidase (SA-β-Gal) positive cells and decreased cell proliferation. Growing research also demonstrates that targeting cellular senescence holds promise in alleviating the progression of IVD degeneration. Long-term systemic or local clearance of senescent cells by senolytic drugs mitigated the age-related IVD degeneration in mice (13) and reduced the expression of pro-inflammatory cytokines and matrix proteases and restored IVD structure in an injury-induced IVD degeneration model in rats (14). Cherif et al. and Mannarino et al. demonstrated that in humans, senolytic drugs o-Vanillin (15) and RG-7112 (16) attenuated NP cellular senescence, where a combination of these two senolytic drugs reduced the release of inflammatory factors and pain mediators in degenerated NP cells from low back pain patients (17).

PDGF is a major constituent of platelet rich plasma (PRP), which is widely used in the clinical setting for tissue regeneration and repair. It can be made of a homodimer of A, B, C, and D polypeptide chains, or an AB heterodimer (18,19). Among these, PDGF-AB and -BB are the predominant forms in PRPs (20). Two types of PDGFR (PDGFRA and PDGFRB) were identified that differ in ligand-binding specificity. PDGFRA binds to all PDGF chains but D chain while PDGFRB only binds to B and D chains (18,19). Upon binding, PDGF-PDGFR network induces a cascade of phosphorylation in pathways including cell proliferation, migration, and survival (21). We previously demonstrated that recombinant human PDGF-BB (rhPDGF-BB) inhibited cell apoptosis while promoting cell proliferation and matrix production in human IVD cells (22). Furthermore, when delivered via hydrogel, rhPDGF-BB successfully inhibited IVD degeneration and restored IVD biomechanical function in a rabbit preclinical model of puncture-induced

109 IVD degeneration (23). In the current study, we hypothesize that PDGF-AB and -BB
110 mitigated IVD degenerating through targeting cellular senescence. To test it, aged,
111 degenerated human IVD cells were treated with rhPDGF-AB or -BB and transcriptome
112 profiling was performed on treated NP and AF cells. We found similar but distinct
113 responses to the treatment between NP and AF cells. In NP cells, PDGF-AB and -BB
114 treatment upregulated the expression of PDGFRA and genes involved in cell cycle
115 progression while downregulating the expression of genes related to ROS production,
116 oxidative stress, and mitochondrial function. The alterations in these pathways indicated
117 that the senescent phenotype was alleviated in human degenerated IVD cells treated
118 with PDGF-AB/BB. Interestingly, in human senescent NP cells induced by irradiation,
119 PDGFRA was significantly reduced while PDGF-AB/BB treatment prevented the
120 progression of senescence through increased cell cycle progression and reduced SA-β-
121 Gal staining and the expression of P21, P16, NF-κB, and IL6. In contrast, AF cells
122 treated with PDGF-AB/BB showed alleviated senescent phenotype independent of
123 PDGFRA.

124 **Methods**

125 **2.1 Sample collection and cell extraction**

126 This study was conducted in accordance with the ethical principles outlined in the
127 Declaration of Helsinki. All experiments and procedures were reviewed and approved by
128 the institutional review board of Emory University (IRB #00099028) approval. Human
129 degenerated NP and AF tissues (Grade IV or V on Pfirrman grade) were obtained from
130 donors after discectomy surgeries for discogenic pain, with each donor providing written

131 informed consent. Healthy NP and AF cells were gifted by Professor Lisbet A. Haglund
132 from McGill University (Tissue Biobank #2019-4896). The donor information was listed
133 in **Table 1**. NP and AF cells were extracted as previously described (24). Isolated cells
134 were expanded in growth medium containing low glucose DMEM, 10% FBS, 1X
135 antibiotic-antimycotic (Thermofisher Scientific, 15240062), and 50 μg/ml L-
136 Ascorbic acid 2-phosphate (Sigma, A8960). Cells were grown at 37°C under 5% CO_2
137 and 20% O_2. To minimize the variability between experiments that may be caused by
138 changes in cell behavior with each passage, cells of passage 3 were used for each
139 experiment.

140

141 **2.2 RNA-sequencing**

142 To synchronize cells and enhance the sensitivity of cells to PDGF stimulation,
143 degenerated NP (n =5/each group) and AF cells (n =6/each group) were serum-
144 deprived in low glucose medium containing 0.2% FBS for 1 day before treating with
145 PDGF-AB (40ng/ml) or -BB (20ng/ml) for 5 days. Total RNA was isolated with TRIzol
146 (ThermoFisher Scientific, 15596018) and purified using miRNeasy kit (Qiagen, 217084).
147 Genomic DNA contamination was eliminated through on-column DNase digestion. The
148 concentration and quality of RNA were determined using Nanodrop and RNA integrity
149 was assessed by Agilent 2200 Bioanalyzer. RNA samples (NP: n = 5, AF: n = 6) with
150 RIN > 7 were shipped in dry ice to Novogene for RNA-sequencing, which was carried
151 out using NovaSeq 6000 (Novogene Corporation Inc). Libraries were constructed from
152 0.2μg RNA using TruSeq Stranded Total RNA Sample Prep Kit (Illumina). Quality control
153 was performed for distribution of sequencing error rate and GC content and data

154 filtering was performed to remove the low-quality reads and reads containing adapters.
155 The resulting sequences were uploaded into the NCBI Sequence Read Archive (SRA)
156 database (PRJNA1150962). The clean reads were mapped to human reference
157 genome sequence using DNASTAR.

158 **2.3 Differential gene expression analysis of RNA-seq data**

159 Unnormalized raw counts exported from DNASTAR were used for pairwise gene
160 expression comparison between untreated and PDGF-AB/BB samples. Differential
161 expression genes (DEGs) were identified using DESeq2 package in R and DEGs with
162 fold change greater than 1.5 and adjusted p value less than 0.05 were considered
163 statistically significant. Heatmap and volcano plots and principal component analysis
164 were performed to visualize the DEGs between untreated and PDGF-AB/BB samples.

165 **2.4 Pathway enrichment analysis**

166 To identify the biological process that DEGs were enriched, Gene ontology (GO)
167 analysis was performed using upregulated and downregulated DEGs separately in R.
168 The significantly enriched GO terms were visualized by dot plot analysis. GeneRatio in
169 X-axis was calculated by the ratio of gene counts enriched in a particular GO term to all
170 the gene counts annotated in the GO term.

171 Gene Set Enrichment Analysis (GSEA) was performed on all the genes to determine
172 whether a predefined set of genes is significantly enriched in untreated or PDGF-BB
173 samples. GSEA was conducted based on KEGG (Kyoto Encyclopedia of Genes and
174 Genomes) database using clusterProfiler package in R(25) and a gene set was
175 considered significantly enriched when the false discovery rate (FDR) was less than

176 0.05. Enrichment score (ES) was calculated to reflect the degree to which a gene set is
177 overrepresented in our dataset, which was ranked based on fold change. Normalized
178 enrichment score (NES) is the ES normalized to the gene set size.

179 **2.5 Protein-protein interaction network analysis**

180 The interactions among DEGs were performed using the Search Tool for the Retrieval
181 of Interacting Genes (STRING) database (v12.0) with an interaction score greater than
182 0.4. Discrete proteins were removed, and the node files were exported and visualized in
183 Cytospace (v3.10.0). To identify essential nodes in the interaction network, the
184 betweenness centrality among the nodes was calculated using CytoNCA plugin (v2.1.6)
185 in Cytospace (26) and the top 10 hub nodes were identified using CyoHubba plugin
186 (v0.1)(27).

187 **2.6 Cellular senescence induction by irradiation**

188 To induce cellular senescence, healthy NP and AF cells (n=4/each group) were exposed
189 to X-ray in a CellRad benchtop X-ray irradiator (Precision X-Ray) at a rate of 2.6
190 Gy/min. The cells were cultured in growth medium and exposed to indicated doses of
191 ionizing radiation (IR) at 50% confluency. Irradiated cells were immediately treated with
192 PDGF-AB/BB (20ng/ml) for 10 days.

193 **2.7 Senescence-associated β-galactosidase (SA-β-Gal) staining**

194 SA-β-Gal staining was performed according to the manufacturer's protocol (Cell
195 Signaling Technology, #9860). In brief, cells cultured in 6-well plates were washed in
196 PBS and fixed with 1X fixative solution for 10 min. 1 ml of β-Gal staining solution
197 (containing 1 mg/ml X-Gal) was added and the cells were incubated at 37 °C in the

198 absence of CO_2 overnight. Cells were washed in PBS and observed under bright-field
199 microscope (ECHO Revolve).

200 **2.8 Immunocytochemistry**

201 Cells cultured on glass coverslips were washed in 1 X PBS and fixed in 4% (v/v)
202 formaldehyde for 10 min. After washing in 1 X PBS, cells were premetallized in PBS
203 with 0.1% Trition X-100 for 15 min. Non-specific binding sites were blocked in 0.1%
204 Tween-20/PBS with 1% bovine serum album for 30 min, followed by incubating with
205 primary antibodies against P21 (1:500, Cell Signaling Technology, #2947), P16 (1:500,
206 Cell Signaling Technology, #80772), or Lamin B1 (1:500, Cell Signaling Technology,
207 #68591S). After overnight incubation at 4 °C, the cells were washed and incubated with
208 the corresponding host-specific secondary antibodies goat anti mouse Alex Fluor 488
209 (1:1000, #ab150113), or goat anti rabbit Alex Fluro 647 (1:1000, #ab150079) for 1 hour.
210 Cells were counterstained and mounted with mounting medium with DAPI (Abcam,
211 #ab104139) and visualized using an Olympus BX63 automated fluorescence
212 microscope.

213 **2.9 Quantitative real-time PCR assays**

214 Total RNA was extracted from cells collected in TRIzol reagent (Thermofisher Scientific,
215 #15596018) and RNA quality was measured using NanoDrop-1000 spectrophotometer
216 (Thermofisher Scientific, #ND-2000). 1μg of RNA was reverse transcribed using Verso
217 cDNA synthesis kit (Thermofisher Scientific, #AB-1453B). Quantification of mRNA
218 expression was determined by SYBR-based real-time PCR using PowerUp SYBR
219 Green Master Mix (Applied Biosystems, #A25742). PCR primer sequences were listed

220 in **Table 2.** Values were normalized to *ACTB*. mRNA levels were presented as fold
221 change compared to untreated cells according to the $2^{-\Delta\Delta CT}$ method.

222 **2.10 Immunoblotting**

223 Whole-cell protein extraction and immunoblotting analysis were performed as previously
224 described (24). Briefly, cells were lysed using RIPA lysis buffer with 1 X protease and
225 phosphatase inhibitor (ThermoFisher Scientific, #PI78440). Protein concentration was
226 determined using Pierce BCA protein assay kit (ThermoFisher Scientific, #23225) and
227 20 μg of cell lysate from each sample was used to determine the protein expression of
228 P21 (1:2000, Cell Signaling Technology, #2947) and NF-kB (1:2000, Cell Signaling
229 Technology, #8242S). All proteins were normalized to b-actin (1:2000, Cell Signaling
230 Technology, #5125S).

231 **2.11 Statistics**

232 One-way analysis of variance (ANOVA) testing was performed to assess the effects of
233 treatment on NP and AF cells with subsequent Dunnett post hoc testing. To analyze the
234 effects of ionizing radiation on the expression of senescence markers in cells, t-test was
235 utilized. The statistical analyses were performed using GraphPad Prism9. A p-value <
236 0.05 was considered statistically significant.

237 **3 Results**

238 **3.1 Transcriptomics of AF and NP cells in response to PDGF-AB/BB**

239 Bulk RNA sequencing was performed to investigate the global changes in gene
240 expression of degenerated AF and NP cells in response to rhPDGF-AB/BB treatment.

241 Principal component analysis (PCA) on all detected genes revealed distinct clusters
242 between untreated and rhPDGF-AB/BB treated samples while clusters of rhPDGF-AB
243 and rhPDGF-BB treated samples were overlapping (**Supplementary figure 1**). As
244 shown in volcano plots, differential expression analysis (|FC|>1.5 and FDR < 0.05)
245 revealed 880 downregulated and 740 upregulated genes in AF cells treated with
246 rhPDGF-AB and 996 downregulated and 821 upregulated genes induced by rhPDGF-
247 BB treatment after 5 days exposure (**Figure 1A**). In contrast, NP cells had 563
248 downregulated and 423 upregulated genes in rhPDGF-AB treated group and 409
249 downregulated and 404 upregulated genes in rhPDGF-BB treated group. The top
250 differentially expressed genes (DEGs) were annotated according to FDR and most of
251 these genes exhibited similarity between treatment groups in both AF and NP cells
252 (**Figure 1A+B**). Furthermore, a heat map visualizing the top 50 DEGs by fold change
253 revealed variability among donors while demonstrating an overall consistent response
254 to rhPDGF-AB/BB treatment across the samples (**Figure 1C+D**). Tissue-specific
255 changes were observed in AF and NP cells when treated with rhPDGF-AB/BB. For
256 example, *SLC26A4* (Pendrin) and *CA2*, regulators of the process of transporting and
257 producing bicarbonate, are involved in the homeostatic control of pH in various type of
258 cells (28,29) and their expression was upregulated in NP cells when treated with
259 rhPDGF-AB/BB (**Figure 1D**). *MAMDC2* and *COL21A1*, involved in extracellular matrix
260 organization (30,31), were also upregulated in NP cells while *WISP2* (32) and
261 *RARRES2* (33), modulators of the induction of inflammatory mediators and immune
262 response, were downregulated after treatment. In contrast, in addition to the commonly
263 upregulated *CA2, MDMC2* and *RARRES2*, AF cells showed alterations in genes

involved in mechanical stress, pain sensation, and angiogenesis, such as *CSRP3* (34), *PI16* (35), *EFEMP1* (36) and *SLC26A4-AS1* (37) (**Figure 1C**). Notably, *PRELP*, potentially associated with Hutchinson-Gilford progeria (38), was also downregulated in rhPDGF-AB/BB treated AF cells (**Figure 1A**).

3.2 Functional analysis of AF cells treated with PDGF-AB/BB

To investigate the enriched biological processes (BP) induced by rhPDGF-AB/BB treatment in AF cells, gene ontology (GO) analysis was performed using upregulated and downregulated DEGs separately. As expected, the biological processes between rhPDGF-AB and -BB treated samples were mostly overlapping (**Figure 2A+B**). In AF cells, upregulated DEGs were significantly enriched in biological processes including regulation of cell cycle and chromosome segregation. Furthermore, AF cells demonstrated upregulated pathways including mesenchymal cell differentiation and response to oxygen levels and downregulated pathways including response to ROS and oxidative stress (**Figure 2A**). Moreover, the treatment downregulated groups of genes related to neurogenesis and response to mechanical stimulus (**Figure 2B**). In line with the results of GO analysis, GSEA analysis revealed an overrepresentation of cell cycle pathway in rhPDGF-AB/BB treated cells (**Figure 2C**). Additionally, the ErbB signaling pathway, proteasome pathway, and cytosolic DNA-sensing pathway were enriched, suggesting that PDGF-AB/BB treatment promoted cell growth, protein turnover, and maintenance of cellular homeostasis. The leading-edge genes that contributed most significantly to these pathways include *CCNB1, CCND1, AREG, PSMB9, TREX1,* and *POLR3A*, as shown in **Figure 2D.**

3.3 Functional analysis of NP cells treated with PDGF-AB/BB

GO analysis revealed similar yet distinct responses to rhPDGF-AB/BB treatment between NP and AF cells. In NP cells**,** rhPDGF-AB and -BB treatment upregulated groups of genes related to cartilage development, cell-matrix adhesion, Wnt signaling pathway, and response to decreased oxygen levels, which were all important to maintaining NP phenotype (**Figure 3A**). Downregulated DEGs were enriched in GO terms associated with fatty acid metabolism, cellular respiration, mitochondrial function, and reactive oxygen species production (**Figure 3B**), suggesting alterations in cellular metabolism and oxidative stress. Gene set enrichment analysis (GSEA) on the entire transcriptomics also revealed that Wnt signaling pathway and neuroactive ligand-receptor interaction were upregulated while the pathways related to oxidative phosphorylation and ribosome were downregulated in rhPDGF-BB treated NP cells (**Figure 3C**). The core enrichment genes associated with these pathways were visualized in a chord diagram (**Figure 3D**). Specifically, the leading-edge DEGs enriched in Wnt signaling pathway include *WNT7B, WNT5A, NKD1*, and *SFRP1* and oxidative phosphorylation pathway showed enrichment in *NDUFB7, NDUFA11, COX5B*, and *CYC1*.

To better understand the regulatory mechanisms of PDGF-AB/BB in degenerated NP cells, DEGs between untreated and treated groups were used to construct protein-protein interaction (PPI) networks through STRING and Cytoscape software. The network of the top 10 hub nodes based on betweenness was demonstrated in **Figure 3E** and it revealed the strong correlation between *PDGFRA (*PDGF receptor alpha) and *IL6, MDM2*, *MDM2*, *CCND1, PIK3R1, NOP53, FN1,* and *IDH2*. The enrichment of hub gene *IDH2*, which plays a role in generating NADPH within mitochondria, further

310 validated the alterations in oxidative phosphorylation pathway and subsequent ROS
311 production, as indicated by GSEA and GO analysis in rhPDGF-AB/BB treated NP cells.
312 *MDM2* (a negative regulator of P53) and predicted *NOP53* (a regulator of P53 binding
313 activity) suggested that PDGF-BB interfered with P53 signaling pathway. The interaction
314 between these genes and inflammatory cytokine *IL6* indicated a potential involvement of
315 PDGF-AB/BB in cellular senescence. The gene expression of top hub genes PDGFRA
316 and IL6 was further verified in both NP (**Figure 3F**) and AF (**Figure 3G**) cells by qPCR.
317 PDGF-AB/BB increased the gene expression of PDGFRA in only NP cells and reduced
318 the IL6 gene expression in both type of cells. Taken together, NP and AF cells
319 responded differently to PDGF-AB/BB treatment, but both cell types showed a positive
320 regulation of cell cycle and inhibited inflammation, response to ROS, oxidative stress,
321 and mitochondrial dysfunction, indicating a role of PDGF-AB/BB in IVD cell senescence.

322 **3.4 Induction of NP cellular senescence through X-ray radiation**

323 To test our hypothesis that PDGF-AB/BB provides protection against the progression of
324 cellular senescence in the IVD, we first created a cellular senescence model using X-
325 ray radiation. The healthy NP cells were exposed to 5, 10 and 15 Gy of irradiation and
326 cultured for 7-10 days to develop senescent phenotype. SA-β-gal staining was
327 performed to detect senescent cells. We found that non-irradiated, proliferating NP cells
328 showed elongated, spindle-shaped morphology and faint SA-β-gal staining at day 7
329 (**Figure 4A**). In contrast, cells exposed to 5 and 10 Gy of irradiation developed
330 characteristics of a senescent cell phenotype — enlarged cell size, low cell number, and
331 a higher percentage of SA-β-gal positive cells. However, cells exposed to 15 Gy of
332 radiation underwent significant cell death, showing negligible SA-β-gal staining. As a

333 result, we excluded the 15 Gy dosage group in subsequent studies. To quantify cell
334 growth, MTT assay was performed, which revealed reduced cell proliferation under 5
335 and 10 Gy of irradiation compared to the non-irradiated group (**Figure 4B**).
336 Furthermore, we examined the expression of senescence related markers — Lamin B1,
337 P21 and P16. Lamin B1 is a structural component of the nucleus, and its loss is a
338 senescence-associated biomarker (39). Non-irradiated cells displayed nuclear Lamin B1
339 expression while its expression was lost in healthy NP cells exposed to 5 and 10 Gy of
340 irradiation for 7 days (**Figure4C**). Meanwhile, nuclear localization of P21 (**Figure 4C**)
341 and P16 (**Figure 4D**) was observed in irradiated cells, with little immunopositivity in non-
342 irradiated cells at day 7. However, the transcripts of *P21* and *P16* were not significantly
343 decreased until day 10 (**Figure 4E+F**). Caspase 3 (*CASP3*) gene expression was
344 reduced at both timepoints, suggesting that the irradiated cells were resistant to
345 apoptosis. Furthermore, the gene expression of *PDGFRA* was significantly decreased in
346 cells under 10 Gy of irradiation at day 10. Taken together, when exposed to irradiation
347 for 10 days, healthy human NP cells developed senescent phenotype, accompanied
348 with decreased PDGFRA expression.

349 **3.5 PDGF-AB/BB inhibited senescent phenotype in NP and AF cells**

350 To investigate the protective effects of PDGF-AB/BB against cell senescence in the IVD,
351 healthy human NP and AF cells were exposed to 10Gy of irradiation, followed by
352 immediate treatment with 20 ng/ml rhPDGF-AB/BB for 10 days. We first examined the
353 cell cycle progression using DAPI stained cells and found that rhPDGF-BB significantly
354 increased the percentage of cell population in the S phase in irradiated NP (**Figure 5A-**
355 **B**) and AF (**Figure 5C-D**) cells at day 10. In rhPDGF-AB treated cells, the percentage of

356 cell population in the S phase was increased in AF cells, but not significantly in NP cells.
357 These findings suggested that PDGF-AB/BB rescued IVD cells from cell cycle arrest in
358 irradiation induced senescent cells. Additionally, SA-β-gal staining demonstrated an
359 increase in the number of senescent cells after irradiation at day 10, whereas a
360 decrease was examined in rhPDGF-AB/BB treated NP and AF cells (**Figure 5E**).

361 At day 10, we analyzed the expression of *PDGFRA* and key senescence regulators of
362 cell cycle inhibitors *P21* and *P16*, *CASP3*, and SASP mediator *IL6.* The treatment of
363 rhPDGF-BB to irradiated NP cells significantly increased the gene expression of
364 *PDGFRA* and decreased the gene expression of *P21*, *P16*, and *IL6*, while playing no
365 effect in the gene expression of *CASP3* **(Figure 6A)**. Comparably, the treatment of
366 rhPDGF-AB to irradiated NP cells significantly decreased the gene expression of *P21*
367 and *IL6* and played no effect on the gene expression of *PDGFRA*, *P16*, and *CASP3*
368 **(Figure 6A)**. In AF cells, the results show that the treatment of rhPDGF-BB and
369 rhPDGF-AB reduced the gene expression of *P21* as those of NP cells **(Figure 6B)**.
370 However, the treatment of either rhPDGF-BB or rhPDGF-AB had no effect in the gene
371 expression of other genes examined **(Figure 6B)**. The lack of change in the gene
372 expression of *PDGFRA* from the treatment of either rhPDGF-BB or rhPDGF-AB
373 suggested that PDGF-BB reduced senescent phenotype through other receptors in AF
374 cells.

375 Furthermore, compared to irradiation only group, the protein levels of P21 and NF-κB, a
376 major regulator stimulating SASP, were inhibited in rhPDGF-BB treated NP cells (**Figure**
377 **6C**). In irradiated AF cells, the protein expression of P21 was significantly reduced by
378 rhPDGF-BB treatment. The expression of NF-kB showed a decreasing trend in

379 rhPDGF-BB treated cells. rhPDGF-AB had no effects on the protein expression of P21
380 and NF-kB. Overall, PDGF-BB mitigated the progression of senescent phenotype in
381 both human NP and AF cells.

382 **Discussion**

383 The current study has shown for the first time that PDGF-AB and -BB treatment not only
384 alleviated the senescent phenotype, but also suppressed the progression of cellular
385 senescence in the IVD. Specifically, in aged, degenerated human NP and AF cells,
386 PDGF-AB/BB treatment suppressed the ROS accumulation, mitochondrial dysfunction,
387 and the resultant oxidative stress, while stimulating cell cycle progression. In the NP,
388 PDGFRA was among the top hub genes that showed strong interaction with other
389 genes. Moreover, its expression was significantly reduced in irradiation induced
390 senescent cells. Importantly, immediate PDGF-BB treatment after irradiation promoted
391 the expression of *PDGFRA* and provided protection to IVD cells against acquiring
392 senescence associated phenotype. This novel function of PDGF-BB/PDGFRA signaling
393 is likely linked to their ability to inhibit NF-κB, P16, and P21 pathways in NP cells. In
394 contrast, PDGF-AB/BB alleviated the senescent phenotype in AF cells independent of
395 PDGFRA.

396 Senescence is a key contributor to the onset and the progression of IVD degeneration
397 (40). It can occur naturally with aging or can be triggered by growth factor deficiency,
398 radiation, DNA damage, oxidative stress, and inflammatory stimuli (41,42). Senescent
399 cells exit the cell cycle and cannot divide; their accumulation reduce the IVD's ability to
400 generate new cells to replace apoptotic or necrotic cells. It has been well established
401 that increased number of senescent cells was positively correlated with the IVD aging

402 and the severity of degeneration while negatively correlated with the percentage of
403 proliferating cells in human NP and AF tissues (10–12). Since PDGF is a mitogenic
404 growth factor and promotes cell proliferation in various cell types (21,43,44), it is
405 intriguing to explore whether PDGF-AB/BB could mitigate or prevent against the cellular
406 senescence in IVDs. We observed groups of upregulated genes regulating cell cycle
407 progression and cell proliferation in PDGF-AB/BB treated NP cells. AF cells also had an
408 upregulation of chromosome segregation and mitotic nuclear division pathways,
409 suggesting that these cells were actively proliferating. Cell cycle progression is
410 controlled by cyclins, and the expression of cyclin D1 and B1, regulators of the G1/S
411 and G2/M phase transition respectively, was increased in degenerated NP cells after
412 PDGF-AB/BB treatment. Transcriptomic analysis also revealed that increased cyclin D1
413 was among the top hub nodes, tightly regulated by PDGF-AB and BB. In addition, cell
414 cycle analysis confirmed that PDGF-AB/BB induced the transition from G1 to S1 phase
415 in senescent IVD cells. Our data suggested that PDGF treatment led to an increase in
416 the proliferation of senescent IVD cells in the S phase likely through cyclin D1 and B1.
417 These findings were in accordance with previous studies showing that PDGF stimulated
418 cell proliferation and cyclin D1 expression in rat mesangial cells(45), rat adventitial
419 fibroblasts (46), and human vascular smooth muscle cells (44).

420 The antisenescence of PDGF has been demonstrated in several studies. For example,
421 PDGF-BB decreased SA-β-gal positive cells and the expression of P53 and P21 while
422 enhancing proliferative potential in senescent human dermal fibroblasts (47) and
423 mesenchymal stem cells (MSCs) derived from immune thrombocytopenia patients (48).
424 PDGF exerts its function by binding to its receptors, thereby triggering a cascade of

425 intracellular signaling events, such as cell proliferation and survival. The PDGF-
426 PDGFRA signaling is often suppressed in premature aged or senescent cells (49–51),
427 suggesting that PDGF signaling dysfunction might be involved in senescence or aging.
428 Notably, our transcriptome data has shown that both PDGF-AB and -BB induced the
429 expression of *PDGFRA* in aged, degenerated NP cells. This autoregulatory loop caused
430 IVD cells to become more sensitive to PDGF treatment and augmented the signaling
431 cascades triggered by PDGF binding, including senescence-associated P21, P16, P53,
432 and NF-κB pathways. In line with this thought, PPI analysis revealed that *PDGFRA*
433 closely interacted with upregulated *MDM2*, a negative regulator of P53. NF-κB signaling
434 is a major signaling pathway that is involved in inflamm-aging (52) and induces the
435 onset of SASP (8), such as IL6, IL8, and CXCL1. In our study, irradiation in NP cells led
436 to decreased *PDGFRA* expression, which impaired the activity of PDGF/PDGRFA
437 signaling. However, PDGF-BB treatment promoted the expression of *PDGFRA* and
438 decreased the expression of *P21, P16,* and *IL6* in senescent NP cells, likely by
439 inhibiting NF-κB signaling. These findings support the idea that PDGF treatment could
440 stimulate the expression of *PDGFRA* and prevent healthy IVD cells from developing
441 senescent phenotype. Further studies using preclinical animal models to validify the
442 protectiveness of PDGF against the onset or progression of senescence in the IVD will
443 offer more robust evidence.

444 Degenerated IVD cells experienced an imbalance between ROS accumulation and
445 antioxidant capacity, leading to oxidative stress, which is involved in cellular senescence
446 (53). Mitochondrion is the primary location of intracellular ROS production and its
447 dysfunction in degenerated IVD cells causes electron leakage, resulting in the formation

448 of superoxide radicals (54). PDGF-AB/BB treatment suppressed the activity of damaged
449 mitochondria, leading to decreased ROS and oxidative stress in degenerated NP and
450 AF cells, as indicated by GO BP analysis. Consistently, GSEA revealed the
451 underrepresentation of oxidative phosphorylation in treated NP cells. The
452 downregulation of genes related to mitochondria activity and oxidative phosphorylation
453 may be indicative of a shift in metabolic pathways, leading cells to potentially prioritize
454 alterative pathways such as glycolysis. Indeed, PDGF treatment upregulated groups of
455 genes involved in response to decreased oxygen levels, suggesting that the treatment
456 activated cellular mechanisms involving in sensing and adapting to low oxygen
457 conditions. In line with this idea, it has been demonstrated that hypoxia-inducible factor
458 1α is highly expressed in healthy NP cells to suppress oxidative phosphorylation and
459 enhanced glycolysis, allowing cells to adjust to a hypoxia microenvironment (55,56).
460 Conversely, degenerated NP cells show an opposite metabolic pattern (55,56).

461 Besides the anti-senescence, NP and AF cells responded differently to PDGF-AB/BB
462 treatment. AF cells were more responsive to the treatment with twice as many DEGs as
463 NP cells. The difference in tissue architecture and cellular contents between NP and AF
464 contributes to their specialized functions (57). The multiple layers of concentric lamellae
465 in the AF enables it to withstand circumferential loads while this highly organized
466 structure was disrupted with aging and degeneration (58). In addition, damage to the AF
467 has the potential to stimulate neovascularization and nerve ingrowth, provoking an
468 inflammatory response and contributing to low back pain. PDGF-AB/BB treatment
469 downregulated groups of genes related to neurogenesis and response to mechanical
470 stimulus in AF cells while downregulated genes in the NP were more associated with

metabolic pathways, providing evidence that the treatment enhanced IVD functionality in different aspects between the two compartments.

Senescence as a central hallmark of aging can be induced by several factors (40). One limitation of this study is that we did not examine the protective effects of PDGF-AB/BB treatment on senescence using other senescence models. In addition, our findings were obtained in vitro experiments, so caution is needed when interpreting our data. Our future work will focus on establishing an appropriate experimental animal model to study the functions of PDGF on cellular senescence.

In this study, we demonstrated a novel function of PDGF in human NP and AF cells. PDGF-AB/BB treatment alleviated oxidative stress and mitochondria dysfunction while stimulating cell cycle progression in degenerated IVD cells. In addition, the treatment protected healthy NP and AF cells against the progression of senescence induced by irradiation. Our results suggest that PDGF-AB/BB could be a promising candidate for preventing or treating IVD degeneration by targeting cellular senescence.

Human ethics and consent to participate:

This study was conducted in accordance with the ethical principles outlined in the Declaration of Helsinki. All experiments and procedures were reviewed and approved by the Institutional Review Board (IRB #00099028) of Emory University for all experimental procedures. Human tissue samples were collected after obtaining familial consent.

Funding statement

Funded by NIH-R01AR076427 to HD, and the Department of Orthopaedics at Emory University School of Medicine.

Acknowledgement

The authors thank Gilbert Gu for his assistance in correcting the grammar in the manuscript.

Conflict of interest:

The authors have no conflict of interest associated with this work.

Authors' contributions:

CZ designed and conducted the study, analyzed and interpreted the data, and drafted the manuscript. TF and MDH reviewed and revised the manuscript. SS assisted in data collection. SY provided diseased IVD tissues and reviewed the manuscript. LH provided healthy IVD cells and revised the manuscript. HD designed the study and interpreted the data. All authors have reviewed the manuscript and provided their consent for publication.

Availability of data and materials:

The datasets and code used and analyzed during the current study are available from the corresponding author on reasonable request.

Figure legends

513 **Figure 1. Transcriptomics of AF and NP cells in response to PDGF-AB/BB**
514 **treatment. A + B**) Volcano plots showing the differentially expressed genes (DEGs) in
515 AF (**A**) and NP (**B**) cells treated with rhPDGF-AB/BB for 5 days (cutoff: |FC| > 1.5 and
516 FDR < 0.05). DEGs were annotated in the plot according to FDR. **C+D)** Heatmap plots
517 showing the top 50 DEGs in rhPDGF-AB/BB treated AF (**C**) and NP (**D**) cells based on
518 fold change. NP: n = 5 samples. AF: n = 6 samples.

519 **Figure 2. Functional analysis of AF cells treated with PDGF-AB/BB. A + B)** Gene
520 ontology (GO) analysis for biological process using upregulated (**A**) and downregulated
521 (**B**) DEGs in AF cells. Y-axis label represents GO terms, and x-axis represents
522 geneRatio (geneRatio refers to the proportion of genes that are annotated in specific
523 GO term within all the input genes). The size of bubble represents the gene counts
524 enriched in a particular GO term and the color indicates the FDR of GO terms. **C)** Gene
525 set enrichment analysis (GSEA) on the entire transcriptome profile demonstrated an
526 upregulation of cell cycle, cytosolic DNA-sensing pathway, ErbB signaling pathway, and
527 proteasome and a downregulation of drug metabolism-cytochrome P450 pathway in
528 rhPDGF-BB treated NP cells. **D**) The leading-edge genes associated with these
529 pathways were shown using a chord diagram.

530 **Figure 3. Functional analysis of NP cells treated with PDGF-AB/BB. A + B)** Gene
531 ontology (GO) analysis for biological process using upregulated **(A)** and downregulated
532 **(B)** DEGs in NP cells. Y-axis label represents GO terms, and x-axis represents
533 geneRatio (geneRatio refers to the proportion of genes that are annotated in specific
534 GO term within all the input genes). The size of bubble represents the gene counts
535 enriched in a particular GO term and the color indicates the FDR of GO terms. **C)** Gene

536 set enrichment analysis (GSEA) on the entire transcriptome profile demonstrated an
537 upregulation of Wnt signaling pathway and a downregulation of oxidative
538 phosphorylation and ribosome in rhPDGF-BB treated NP cells. **D)** The leading-edge
539 genes associated with these pathways were shown using a chord diagram. **E)** Protein-
540 protein interaction network using DEGs was constructed in STRING and visualized in
541 Cytospace. **F+G)** The changes in the gene expression of PDGFRA and IL6 were
542 verified in NP **(F)** and AF **(G)** cells treated with rhPDGF-AB (40ng/ml) or -BB (20ng/ml)
543 for 5 days. *p< 0.05. **p< 0.01. ***p< 0.001.

544 **Figure 4. Cellular senescence induction by irradiation**. **A)** SA-β-gal staining in
545 healthy NP cells under different doses of irradiation at day 7. **B)** MTT assay showed
546 decreased cell proliferation after irradiation at day 7. **C, D**) Immunocytochemistry
547 staining on Lamin B1 and P21 (**C**) and P16 (**D**) in irradiated cells at day 7. Scale bar =
548 100uM. **E)** Changes in the gene expression levels of *P21, P16,* and *CASP3* in NP cells
549 under 10 Gy of irradiation at day 7. **F**) The gene expression of *P21, P16, CASP3, IL6,*
550 *and* PDGFRA was altered in NP cells under 10 Gy of irradiation at day 10. n = 4 per
551 group. Statistical significance is analyzed using t-test. The data is presented as mean
552 with SD. **p*< 0.05. ***p*< 0.001. ****p*< 0.0001.

553 **Figure 5. PDGF-AB/BB treatment protected healthy NP and AF cells against**
554 **senescence progression**. **A-F)** Cell cycle analysis by DAPI staining in irradiated
555 healthy NP (**A-B)** and AF (**C-D)** cells treated with rhPDGF-AB/BB for 10days. The upper
556 panel shows the data obtained from NP cells, and lower panel shows the data from AF
557 cells. Representative graphs (**A+C)** showing the changes in cell cycle progression in NP
558 and AF cells after treatment. Quantification of cell cycle analysis showed the cell

559 percentage in each phase (**B+D**). **E)** SA-β-gal staining in irradiated healthy NP (upper
560 panel) and AF cells (lower panel) showing the reduced SA-β-gal positive cells after
561 treatment. Scale bar = 100uM. Two-way ANOVA with Dunnett post hoc testing was
562 performed. n = 4 each group. The data is presented as mean with SD. *p< 0.05.

563 **Figure 6. PDGF-AB/BB treatment suppressed the expression of senescence**
564 **associated regulators**. **A-B)** Changes in the gene expression of *PDGFRA*, *P21, P16,*
565 *CASP3,* and *IL6* in irradiated NP (**A)** and AF (**B)** cells treated with rhPDGF-AB/BB. **C+D)**
566 Protein expression levels of P21 and NF-κB in irradiated NP (**C)** and AF (**D)** cells treated
567 with rhPDGF-AB/BB. n = 4 each group. One-way ANOVA with Dunnett post hoc testing
568 was performed. The data is presented as mean with SD. *p< 0.05. **p< 0.01. ****p<
569 0.0001.

570

571 **Supplementary figure 1: Principle component analysis (PCA) of NP and AF**
572 **samples treated with rhPDGF-AB and BB. A+B)** PCA plot of NP (**A**) cells and AF cell
573 (**B**) showed the distinct cluster between untreated and treated samples. The clusters of
574 PDGF-AB and BB samples were overlapping. NP: n = 5 each group. AF: n = 6 each
575 group.

576

577

578 **Table captions**

579 **Table 1:** Donor information.

Table 1. Donor information

Grade	Age	Sex	Cell type
4	67	M	NP & AF
5	61	M	NP & AF
5	61	M	NP & AF
4 or 5	65	F	NP & AF
4 or 5	81	F	AF
4	53	F	AF
4	64	F	NP
1	19	M	NP & AF
1	21	M	NP & AF
1	25	F	NP & AF
1	27	F	NP & AF

Table 2: Sequence of primers.

Table 2. Sequence of primers

Gene	Primer sequence
P21	Forward: 5'-GAC ACCACT GGA GGG TGA CT-3' Reverse: 5'-CAGGTC CAC ATG GTC TTC CT-3'
P16	Forward: 5'-CCAACGCACCGAATAGTTACG-3' Reverse: 5'-GCGCTGCCCATCATCATG-3'
IL6	Forward: 5'-CCGGGAACGAAAGAGAAGCT-3' Reverse: 5'-GCGCTTGTGGAGAAGGAGTT-3'
CCNB1	Forward: 5'-ACTGGGTCGGGAAGTCACTG-3' Reverse: 5'-CATTCTTAGCCAGGTGCTGC-3'
CCND1	Forward: 5'-CTGTGCTGCGAAGTGGAAAC-3' Reverse: 5'-TCTGTTTGTTCTCCTCCGCC-3'
CASP3	Forward: 5'-TGG TTC ATC CAG TCG CTT TG-3' Reverse: 5'-ATT CTG TTG CCA CCT TTC G-3'
MKI67	Forward: 5'-ATTTGCTTCTGGCCTTCCCC-3' Reverse: 5'-CCAAACAAGCAGGTGCTGAG-3'
ACTB	Forward: 5'-CTC TTC CAG CCT TCC TTC CT-3' Reverse: 5'-AGC ACT GTG TTG GCG TAC AG-3'
PDGFRA	Forward: 5'-AGAAAACAACAGCGGCCTTT -3' Reverse: 5'-CTACATCTGGGTCTGGCACA -3'

References

1. Feng Y, Egan B, Wang J. Genetic factors in intervertebral disc degeneration. Genes Dis. 2016 Sep;3(3):178–85.

2. Xin J, Wang Y, Zheng Z, Wang S, Na S, Zhang S. Treatment of intervertebral disc degeneration. Orthop Surg. 2022 Jul;14(7):1271–80.

3. Coronado RA, George SZ, Devin CJ, Wegener ST, Archer KR. Pain sensitivity and pain catastrophizing are associated with persistent pain and disability after lumbar spine surgery. Arch Phys Med Rehabil. 2015 Oct;96(10):1763–70.

4. Sivan SS, Wachtel E, Roughley P. Structure, function, aging and turnover of aggrecan in the intervertebral disc. Biochim Biophys Acta. 2014 Oct;1840(10):3181–9.

5. Pattappa G, Li Z, Peroglio M, Wismer N, Alini M, Grad S. Diversity of intervertebral disc cells: phenotype and function. J Anat. 2012 Dec;221(6):480–96.

6. Ngo K, Patil P, McGowan SJ, Niedernhofer LJ, Robbins PD, Kang J, et al. Senescent intervertebral disc cells exhibit perturbed matrix homeostasis phenotype. Mech Ageing Dev. 2017 Sep;166:16–23.

7. Reimann M, Lee S, Schmitt CA. Cellular senescence: Neither irreversible nor reversible. J Exp Med. 2024 Apr 1;221(4).

8. Salminen A, Kauppinen A, Kaarniranta K. Emerging role of NF-κB signaling in

620 the induction of senescence-associated secretory phenotype (SASP). Cell
621 Signal. 2012 Apr;24(4):835–45.

622 9. Kumari R, Jat P. Mechanisms of cellular senescence: cell cycle arrest and
623 senescence associated secretory phenotype. Front Cell Dev Biol. 2021 Mar
624 29;9:645593.

625 10. Veroutis D, Kouroumalis A, Lagopati N, Polyzou A, Chamilos C, Papadodima S,
626 et al. Evaluation of senescent cells in intervertebral discs by lipofuscin staining.
627 Mech Ageing Dev. 2021 Oct;199:111564.

628 11. Gruber HE, Ingram JA, Davis DE, Hanley EN. Increased cell senescence is
629 associated with decreased cell proliferation in vivo in the degenerating human
630 annulus. Spine J. 2009 Mar;9(3):210–5.

631 12. Gruber HE, Ingram JA, Norton HJ, Hanley EN. Senescence in cells of the aging
632 and degenerating intervertebral disc: immunolocalization of senescence-
633 associated beta-galactosidase in human and sand rat discs. Spine. 2007 Feb
634 1;32(3):321–7.

635 13. Novais EJ, Tran VA, Johnston SN, Darris KR, Roupas AJ, Sessions GA, et al.
636 Long-term treatment with senolytic drugs Dasatinib and Quercetin ameliorates
637 age-dependent intervertebral disc degeneration in mice. Nat Commun. 2021 Sep
638 3;12(1):5213.

639 14. Lim S, An SB, Jung M, Joshi HP, Kumar H, Kim C, et al. Local delivery of
640 senolytic drug inhibits intervertebral disc degeneration and restores intervertebral

641 disc structure. Adv Healthc Mater. 2022 Jan;11(2):e2101483.

642 15. Mannarino M, Cherif H, Li L, Sheng K, Rabau O, Jarzem P, et al. Toll-like
643 receptor 2 induced senescence in intervertebral disc cells of patients with back
644 pain can be attenuated by o-vanillin. Arthritis Res Ther. 2021 Apr 16;23(1):117.

645 16. Cherif H, Bisson DG, Mannarino M, Rabau O, Ouellet JA, Haglund L.
646 Senotherapeutic drugs for human intervertebral disc degeneration and low back
647 pain. eLife. 2020 Aug 21;9.

648 17. Mannarino M, Wu-Martinez O, Sheng K, Li L, Navarro-Ramirez R, Jarzem P, et
649 al. Senolytic Combination Treatment Is More Potent Than Single Drugs in
650 Reducing Inflammatory and Senescence Burden in Cells from Painful
651 Degenerating IVDs. Biomolecules. 2023 Aug 16;13(8).

652 18. Chen P-H, Chen X, He X. Platelet-derived growth factors and their receptors:
653 structural and functional perspectives. Biochim Biophys Acta. 2013
654 Oct;1834(10):2176–86.

655 19. Heldin C-H, Lennartsson J. Structural and functional properties of platelet-
656 derived growth factor and stem cell factor receptors. Cold Spring Harb Perspect
657 Biol. 2013 Aug 1;5(8):a009100.

658 20. Weibrich G, Kleis WKG, Hafner G, Hitzler WE. Growth factor levels in platelet-
659 rich plasma and correlations with donor age, sex, and platelet count. J
660 Craniomaxillofac Surg. 2002 Apr;30(2):97–102.

661 21. Contreras O, Córdova-Casanova A, Brandan E. PDGF-PDGFR network
662 differentially regulates the fate, migration, proliferation, and cell cycle progression
663 of myogenic cells. Cell Signal. 2021 Aug;84:110036.

664 22. Presciutti SM, Paglia DN, Karukonda T, Soung DY, Guzzo R, Drissi H, et al.
665 PDGF-BB inhibits intervertebral disc cell apoptosis in vitro. J Orthop Res. 2014
666 Sep;32(9):1181–8.

667 23. Paglia DN, Singh H, Karukonda T, Drissi H, Moss IL. PDGF-BB Delays
668 Degeneration of the Intervertebral Discs in a Rabbit Preclinical Model. Spine.
669 2016 Apr;41(8):E449-58.

670 24. Zhang C, Gordon MD, Joseph KM, Diaz-Hernandez ME, Drissi H, Illien-Jünger
671 S. Differential efficacy of two small molecule PHLPP inhibitors to promote
672 nucleus Pulposus cell health. JOR Spine. 2024 Mar;7(1):e1306.

673 25. Wu T, Hu E, Xu S, Chen M, Guo P, Dai Z, et al. clusterProfiler 4.0: A universal
674 enrichment tool for interpreting omics data. Innovation (Camb). 2021 Aug
675 28;2(3):100141.

676 26. Tang Y, Li M, Wang J, Pan Y, Wu F-X. CytoNCA: a cytoscape plugin for centrality
677 analysis and evaluation of protein interaction networks. BioSystems. 2015
678 Jan;127:67–72.

679 27. Chin C-H, Chen S-H, Wu H-H, Ho C-W, Ko M-T, Lin C-Y. cytoHubba: identifying
680 hub objects and sub-networks from complex interactome. BMC Syst Biol. 2014
681 Dec 8;8 Suppl 4(Suppl 4):S11.

682 28. Vince JW, Reithmeier RA. Carbonic anhydrase II binds to the carboxyl terminus
683 of human band 3, the erythrocyte C1-/HCO3- exchanger. J Biol Chem. 1998 Oct
684 23;273(43):28430–7.

685 29. Silagi ES, Schoepflin ZR, Seifert EL, Merceron C, Schipani E, Shapiro IM, et al.
686 Bicarbonate Recycling by HIF-1-Dependent Carbonic Anhydrase Isoforms 9 and
687 12 Is Critical in Maintaining Intracellular pH and Viability of Nucleus Pulposus
688 Cells. J Bone Miner Res. 2018 Feb;33(2):338–55.

689 30. Chou M-Y, Li H-C. Genomic organization and characterization of the human type
690 XXI collagen (COL21A1) gene. Genomics. 2002 Mar;79(3):395–401.

691 31. Mavillard F, Servian-Morilla E, Dofash L, Rojas-Marcos I, Folland C, Monahan G,
692 et al. Ablation of the carboxy-terminal end of MAMDC2 causes a distinct
693 muscular dystrophy. Brain. 2023 Dec 1;146(12):5235–48.

694 32. Ruiz-Fernández C, González-Rodríguez M, Abella V, Francisco V, Cordero-
695 Barreal A, Ait Eldjoudi D, et al. WISP-2 modulates the induction of inflammatory
696 mediators and cartilage catabolism in chondrocytes. Lab Invest. 2022
697 Sep;102(9):989–99.

698 33. Liu-Chittenden Y, Jain M, Gaskins K, Wang S, Merino MJ, Kotian S, et al.
699 RARRES2 functions as a tumor suppressor by promoting β-catenin
700 phosphorylation/degradation and inhibiting p38 phosphorylation in adrenocortical
701 carcinoma. Oncogene. 2017 Jun 22;36(25):3541–52.

702 34. Rashid MM, Runci A, Russo MA, Tafani M. Muscle Lim Protein (MLP)/CSRP3 at

703 the crossroad between mechanotransduction and autophagy. Cell Death Dis.
704 2015 Oct 22;6(10):e1940.

705 35. Singhmar P, Trinh RTP, Ma J, Huo X, Peng B, Heijnen CJ, et al. The fibroblast-
706 derived protein PI16 controls neuropathic pain. Proc Natl Acad Sci USA. 2020
707 Mar 10;117(10):5463–71.

708 36. Song E-L, Hou Y-P, Yu S-P, Chen S-G, Huang J-T, Luo T, et al. EFEMP1
709 expression promotes angiogenesis and accelerates the growth of cervical cancer
710 in vivo. Gynecol Oncol. 2011 Apr;121(1):174–80.

711 37. Li H, Yan R, Chen W, Ding X, Liu J, Chen G, et al. Long non coding RNA
712 SLC26A4-AS1 exerts antiangiogenic effects in human glioma by upregulating
713 NPTX1 via NFKB1 transcriptional factor. FEBS J. 2021 Jan;288(1):212–28.

714 38. Lewis M. PRELP, collagen, and a theory of Hutchinson-Gilford progeria. Ageing
715 Res Rev. 2003 Jan;2(1):95–105.

716 39. Freund A, Laberge R-M, Demaria M, Campisi J. Lamin B1 loss is a senescence-
717 associated biomarker. Mol Biol Cell. 2012 Jun;23(11):2066–75.

718 40. Silwal P, Nguyen-Thai AM, Mohammad HA, Wang Y, Robbins PD, Lee JY, et al.
719 Cellular senescence in intervertebral disc aging and degeneration: molecular
720 mechanisms and potential therapeutic opportunities. Biomolecules. 2023 Apr
721 18;13(4).

722 41. Wang F, Cai F, Shi R, Wang XH, Wu XT. Aging and age related stresses: a

723 senescence mechanism of intervertebral disc degeneration. Osteoarthr Cartil.
724 2016 Mar;24(3):398–408.

725 42. Huang W, Hickson LJ, Eirin A, Kirkland JL, Lerman LO. Cellular senescence: the
726 good, the bad and the unknown. Nat Rev Nephrol. 2022 Oct;18(10):611–27.

727 43. García-Olivas R, Vilaró S, Reina M, Castel S. PDGF-stimulated cell proliferation
728 and migration of human arterial smooth muscle cells. Colocalization of PDGF
729 isoforms with glycosaminoglycans. Int J Biochem Cell Biol. 2007 May
730 25;39(10):1915–29.

731 44. Martin-Garrido A, Williams HC, Lee M, Seidel-Rogol B, Ci X, Dong J-T, et al.
732 Transforming growth factor β inhibits platelet derived growth factor-induced
733 vascular smooth muscle cell proliferation via Akt-independent, Smad-mediated
734 cyclin D1 downregulation. PLoS ONE. 2013 Nov 13;8(11):e79657.

735 45. Hida M, Fujita H, Ishikura K, Omori S, Hoshiya M, Awazu M. Eicosapentaenoic
736 acid inhibits PDGF-induced mitogenesis and cyclin D1 expression via TGF-beta
737 in mesangial cells. J Cell Physiol. 2003 Aug;196(2):293–300.

738 46. Chen J, Wei J-Q, Hong M-N, Zhang Z, Zhou H-D, Lu Y-Y, et al. Mitogen-
739 Activated Protein Kinases Mediate Adventitial Fibroblast Activation and
740 Neointima Formation via GATA4/Cyclin D1 Axis. Cardiovasc Drugs Ther. 2023
741 Jan 18;

742 47. Bae Y-U, Choi J-H, Nagy A, Sung H-K, Kim J-R. Antisenescence effect of mouse
743 embryonic stem cell conditioned medium through a PDGF/FGF pathway. FASEB

744 J. 2016 Mar;30(3):1276–86.

745 48. Zhang J-M, Feng F-E, Wang Q-M, Zhu X-L, Fu H-X, Xu L-P, et al. Platelet-
746 Derived Growth Factor-BB Protects Mesenchymal Stem Cells (MSCs) Derived
747 From Immune Thrombocytopenia Patients Against Apoptosis and Senescence
748 and Maintains MSC-Mediated Immunosuppression. Stem Cells Transl Med. 2016
749 Dec;5(12):1631–43.

750 49. Tan J-K, Jaafar F, Makpol S. Proteomic profiling of senescent human diploid
751 fibroblasts treated with gamma-tocotrienol. BMC Complement Altern Med. 2018
752 Nov 29;18(1):314.

753 50. Pan C-H, Chen C-J, Shih C-M, Wang M-F, Wang J-Y, Wu C-H. Oxidative stress-
754 induced cellular senescence desensitizes cell growth and migration of vascular
755 smooth muscle cells through down-regulation of platelet-derived growth factor
756 receptor-beta. Aging (Albany NY). 2019 Oct 3;11(19):8085–102.

757 51. Mori S, Kawano M, Kanzaki T, Morisaki N, Saito Y, Yoshida S. Decreased
758 expression of the platelet-derived growth factor beta-receptor in fibroblasts from
759 a patient with Werner's syndrome. Eur J Clin Invest. 1993 Mar;23(3):161–5.

760 52. Songkiatisak P, Rahman SMT, Aqdas M, Sung M-H. NF-κB, a culprit of both
761 inflamm-ageing and declining immunity? Immun Ageing. 2022 May 17;19(1):20.

762 53. Feng C, Yang M, Lan M, Liu C, Zhang Y, Huang B, et al. ROS: crucial
763 intermediators in the pathogenesis of intervertebral disc degeneration. Oxid Med
764 Cell Longev. 2017 Mar 14;2017:5601593.

54. Wang D-K, Zheng H-L, Zhou W-S, Duan Z-W, Jiang S-D, Li B, et al. Mitochondrial Dysfunction in Oxidative Stress-Mediated Intervertebral Disc Degeneration. Orthop Surg. 2022 Aug;14(8):1569–82.

55. Song C, Hu P, Peng R, Li F, Fang Z, Xu Y. Bioenergetic dysfunction in the pathogenesis of intervertebral disc degeneration. Pharmacol Res. 2024 Apr;202:107119.

56. Silagi ES, Schipani E, Shapiro IM, Risbud MV. The role of HIF proteins in maintaining the metabolic health of the intervertebral disc. Nat Rev Rheumatol. 2021 Jul;17(7):426–39.

57. Kudelko M, Chen P, Tam V, Zhang Y, Kong O-Y, Sharma R, et al. PRIMUS: Comprehensive proteomics of mouse intervertebral discs that inform novel biology and relevance to human disease modelling. Matrix Biology Plus. 2021 Dec;12:100082.

58. Dittmar R, van Rijsbergen MM, Ito K. Moderately degenerated human intervertebral disks exhibit a less geometrically specific collagen fiber orientation distribution. Global Spine J. 2016 Aug;6(5):439–46.

785

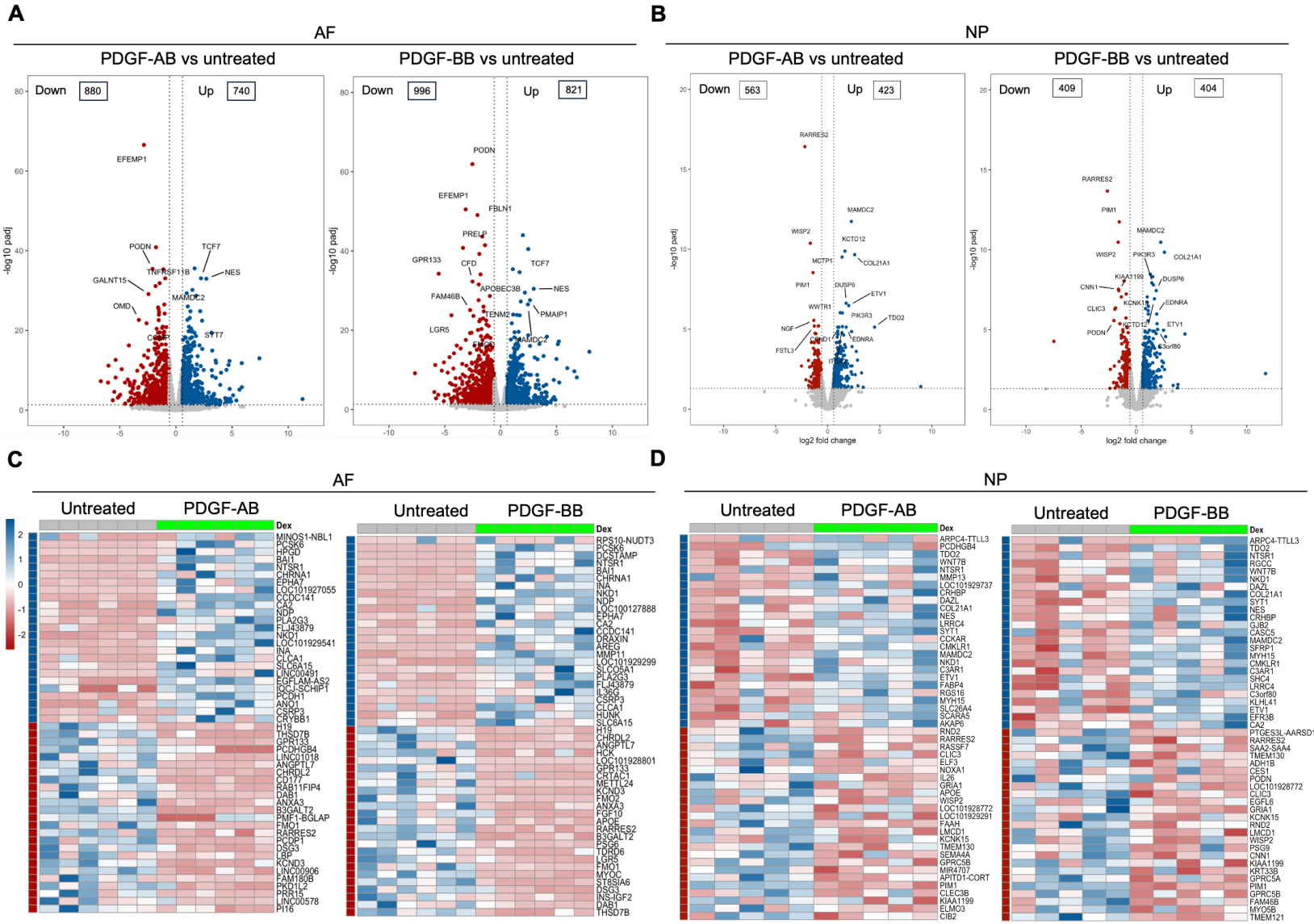
A
AF
PDGF-AB vs untreated
Down 880
Up 740
EFEMP1
PODN
TCF7
TNFRSF11B
NES
GALNT15
MAMDC2
OMD
SYT7
PDGF-BB vs untreated
Down 996
Up 821
PODN
EFEMP1
FBLN1
PRELP
GPR133
CFD
TCF7
APOBEC3B
NES
FAM46B
PMAIP1
TENM2
LGR5
MAMDC2
-log10 padj
B
NP
PDGF-AB vs untreated
Down 563
Up 423
RARRES2
MAMDC2
WISP2
KCTD12
MCTP1
COL21A1
PIM1
DUSP6
ETV1
WWTR1
PIK3R3
TDO2
NGF
EDNRA
FSTL3
PDGF-BB vs untreated
Down 409
Up 404
RARRES2
PIM1
MAMDC2
WISP2
PIK3R3
COL21A1
KIAA1199
DUSP6
CNN1
KCNK15
EDNRA
CLIC3
KCTD12
ETV1
PODN
C3orf80
log2 fold change
C
AF
Untreated
PDGF-AB
Dex
MINOS1-NBL1
PCSK6
HPGD
BAI1
NTSR1
CHRNA1
EPHA7
LOC101927055
CCDC141
CA2
NDP
PLA2G3
FLJ43879
NKD1
LOC101929541
INA
CLCA1
SLC6A15
LINC00491
EGFLAM-AS2
DGCL-SCHIP1
PCDH1
ANO1
CSRP3
CRYBB1
H19
THSD7B
GPR133
PCDHGB4
LINC01018
ANGPTL7
CHRDL2
CD177
RAB11FIP4
DAB1
ANXA3
B3GALT2
PMF1-BGLAP
FMO1
RARRES2
PCDP1
DSG3
LBP
KCND3
LINC00906
FAM180B
PKD1L2
PRR15
LINC00578
PI16
Untreated
PDGF-BB
Dex
RPS10-NUDT3
PCSK6
DCSTAMP
NTSR1
BAI1
CHRNA1
INA
NKD1
NDP
LOC100127888
EPHA7
CA2
CCDC141
DRAXIN
AREG
MMP11
LOC101929299
SLC05A1
PLA2G3
FLJ43879
IL36G
CSRP3
CLCA1
HUNK
SLC6A15
H19
CHRDL2
ANGPTL7
HCK
LOC101928801
GPR133
CRTAC1
METTL24
KCND3
FMO2
ANXA3
FGF10
APOE
RARRES2
B3GALT2
PSG9
TDRD6
LGR5
FMO1
MYOC
ST8SIA6
DSG3
INS-IGF2
DAB1
THSD7B
D
NP
Untreated
PDGF-AB
Dex
ARPC4-TTLL3
PCDHGB4
TDO2
WNT7B
NTSR1
MMP13
LOC101929737
CRHBP
DAZL
COL21A1
NES
LRRC4
SYT1
CCKAR
CMKLR1
MAMDC2
NKD1
C3AR1
ETV1
FABP4
RGS16
MYH15
SLC26A4
SCARA5
AKAP6
RND2
RARRES2
RASSF7
CLIC3
ELF3
NOXA1
IL26
GRIA1
APOE
WISP2
LOC101928772
LOC101929291
FAAH
LMCD1
KCNK15
TMEM130
SEMA4A
GPRC5B
MIR4707
APITD1-CORT
PIM1
CLEC3B
KIAA1199
ELMO3
CIB2
Untreated
PDGF-BB
Dex
ARPC4-TTLL3
TDO2
NTSR1
RGCC
WNT7B
NKD1
DAZL
COL21A1
SYT1
NES
CRHBP
GJB2
CASC5
MAMDC2
SFRP1
MYH15
CMKLR1
C3AR1
SHC4
LRRC4
C3orf80
KLHL41
ETV1
EFR3B
CA2
PTGES3L-AARSD1
RARRES2
SAA2-SAA4
TMEM130
ADH1B
CES1
PODN
LOC101928772
CLIC3
EGFL6
GRIA1
KCNK15
RND2
LMCD1
WISP2
PSG9
CNN1
KIAA1199
KRT33B
GPRC5A
PIM1
GPRC5B
FAM46B
MYO5B
TMEM121

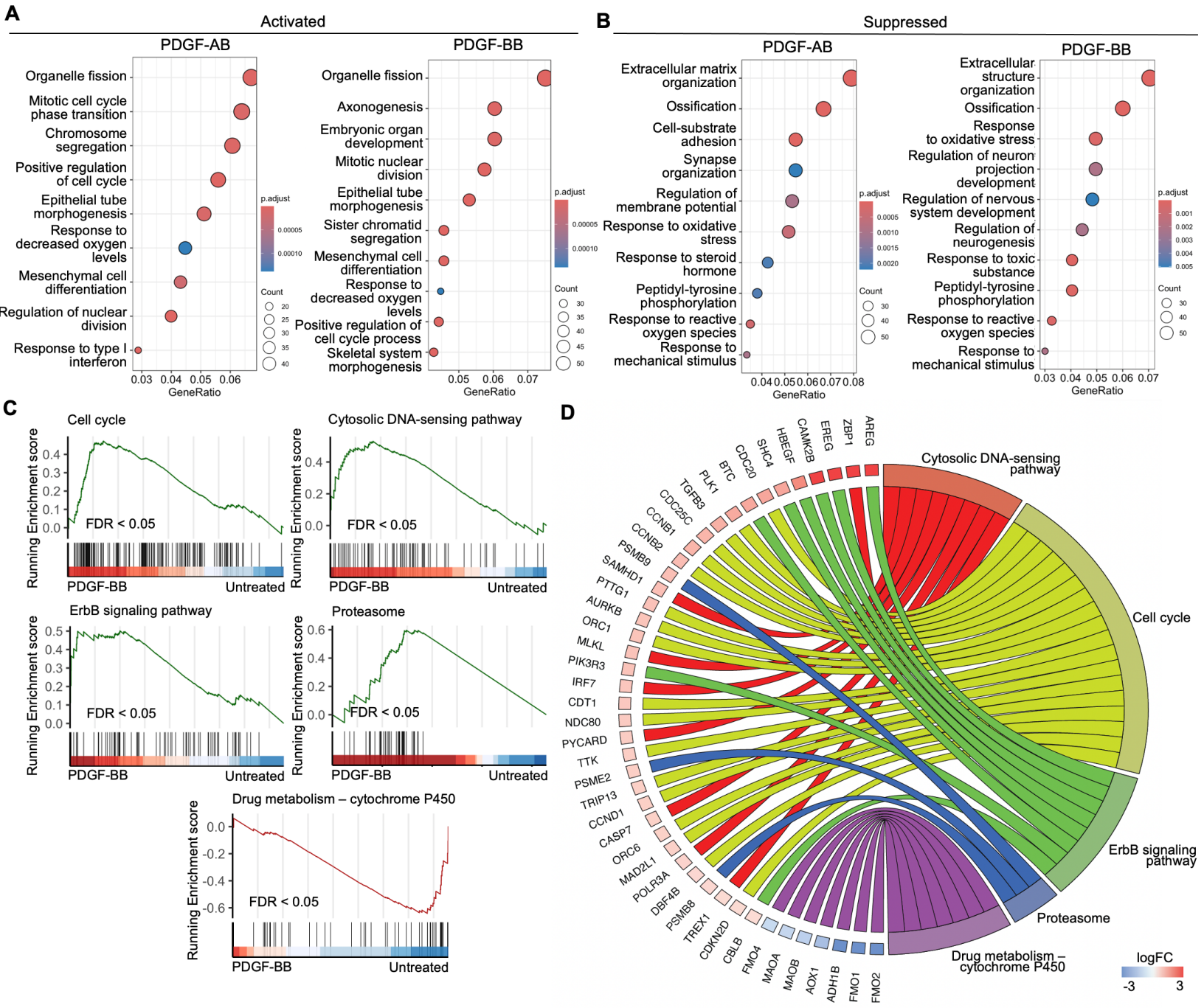
A
Activated
PDGF-AB
Organelle fission
Mitotic cell cycle phase transition
Chromosome segregation
Positive regulation of cell cycle
Epithelial tube morphogenesis
Response to decreased oxygen levels
Mesenchymal cell differentiation
Regulation of nuclear division
Response to type I interferon
GeneRatio
PDGF-BB
Organelle fission
Axonogenesis
Embryonic organ development
Mitotic nuclear division
Epithelial tube morphogenesis
Sister chromatid segregation
Mesenchymal cell differentiation
Response to decreased oxygen levels
Positive regulation of cell cycle process
Skeletal system morphogenesis
p.adjust
Count
B
Suppressed
PDGF-AB
Extracellular matrix organization
Ossification
Cell-substrate adhesion
Synapse organization
Regulation of membrane potential
Response to oxidative stress
Response to steroid hormone
Peptidyl-tyrosine phosphorylation
Response to reactive oxygen species
Response to mechanical stimulus
PDGF-BB
Extracellular structure organization
Ossification
Response to oxidative stress
Regulation of neuron projection development
Regulation of nervous system development
Regulation of neurogenesis
Response to toxic substance
Peptidyl-tyrosine phosphorylation
Response to reactive oxygen species
Response to mechanical stimulus
C
Cell cycle
Cytosolic DNA-sensing pathway
ErbB signaling pathway
Proteasome
Drug metabolism – cytochrome P450
Running Enrichment score
FDR < 0.05
PDGF-BB
Untreated
D
Cytosolic DNA-sensing pathway
Cell cycle
ErbB signaling pathway
Proteasome
Drug metabolism – cytochrome P450
AREG
ZBP1
EREG
CAMK2B
HBEGF
SHC4
CDC20
BTC
PLK1
TGFB3
CDC25C
CCNB1
CCNB2
PSMB9
SAMHD1
PTTG1
AURKB
ORC1
MLKL
PIK3R3
IRF7
CDT1
NDC80
PYCARD
TTK
PSME2
TRIP13
CCND1
CASP7
ORC6
MAD2L1
POLR3A
DBF4B
PSMB8
TREX1
CDKN2D
CBLB
FMO4
MAOA
MAOB
AOX1
ADH1B
FMO1
FMO2
logFC
-3
3

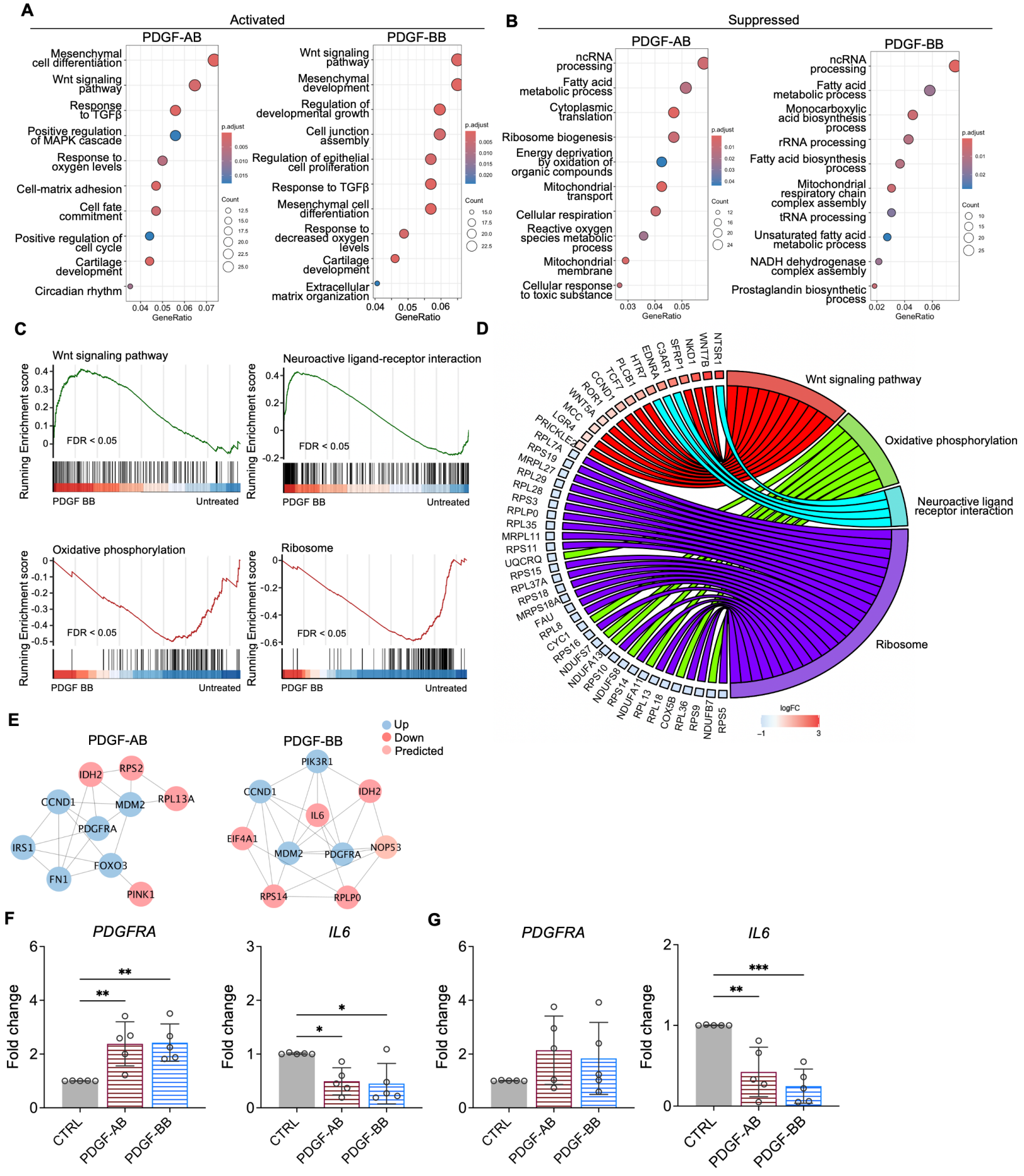
A
Activated
PDGF-AB
Mesenchymal cell differentiation
Wnt signaling pathway
Response to TGFβ
Positive regulation of MAPK cascade
Response to oxygen levels
Cell-matrix adhesion
Cell fate commitment
Positive regulation of cell cycle
Cartilage development
Circadian rhythm
GeneRatio
PDGF-BB
Wnt signaling pathway
Mesenchymal development
Regulation of developmental growth
Cell junction assembly
Regulation of epithelial cell proliferation
Response to TGFβ
Mesenchymal cell differentiation
Response to decreased oxygen levels
Cartilage development
Extracellular matrix organization
p.adjust
Count
B
Suppressed
PDGF-AB
ncRNA processing
Fatty acid metabolic process
Cytoplasmic translation
Ribosome biogenesis
Energy deprivation by oxidation of organic compounds
Mitochondrial transport
Cellular respiration
Reactive oxygen species metabolic process
Mitochondrial membrane
Cellular response to toxic substance
PDGF-BB
ncRNA processing
Fatty acid metabolic process
Monocarboxylic acid biosynthesis process
rRNA processing
Fatty acid biosynthesis process
Mitochondrial respiratory chain complex assembly
tRNA processing
Unsaturated fatty acid metabolic process
NADH dehydrogenase complex assembly
Prostaglandin biosynthetic process
C
Wnt signaling pathway
Neuroactive ligand-receptor interaction
Oxidative phosphorylation
Ribosome
Running Enrichment score
FDR < 0.05
PDGF BB
Untreated
D
Wnt signaling pathway
Oxidative phosphorylation
Neuroactive ligand receptor interaction
Ribosome
NTSR1
WNT7B
NKD1
SFRP1
C3AR1
EDNRA
HTR7
PLCB1
TCF7
CCND1
ROR1
WNT5A
MCC
LGR4
PRICKLE2
RPL7A
RPS19
MRPL27
RPL29
RPL28
RPS3
RPLP0
RPL35
MRPL11
RPS11
UQCRQ
RPS15
RPL37A
RPS18
MRPS18A
FAU
RPL8
CYC1
RPS16
NDUFS7
NDUFA13
RPS10
NDUFS8
RPS14
NDUFA11
RPL13
RPL18
COX5B
RPL36
RPS9
NDUFB7
RPS5
logFC
E
Up
Down
Predicted
PDGF-AB
IDH2
RPS2
CCND1
MDM2
RPL13A
PDGFRA
IRS1
FOXO3
FN1
PINK1
PDGF-BB
PIK3R1
CCND1
IDH2
IL6
EIF4A1
MDM2
PDGFRA
NOP53
RPS14
RPLP0
F
PDGFRA
IL6
Fold change
CTRL
PDGF-AB
PDGF-BB
G
PDGFRA
IL6
Fold change
CTRL
PDGF-AB
PDGF-BB

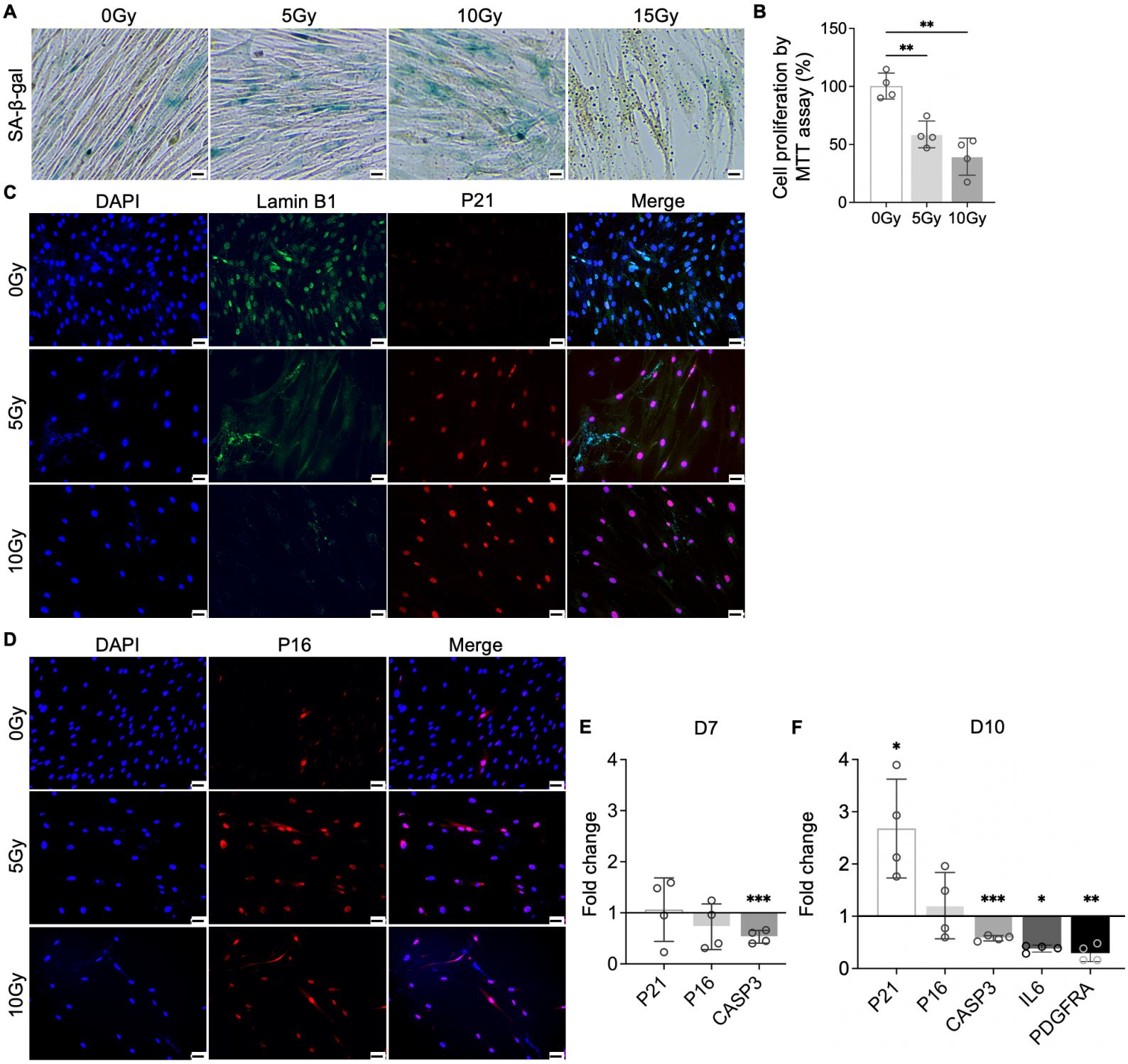
A
0Gy
5Gy
10Gy
15Gy
SA-β-gal
B
Cell proliferation by MTT assay (%)
150
100
50
0
**
**
0Gy
5Gy
10Gy
C
DAPI
Lamin B1
P21
Merge
0Gy
5Gy
10Gy
D
DAPI
P16
Merge
0Gy
5Gy
10Gy
E
D7
Fold change
4
3
2
1
0
***
P21
P16
CASP3
F
D10
Fold change
4
3
2
1
0
*
***
*
**
P21
P16
CASP3
IL6
PDGFRA

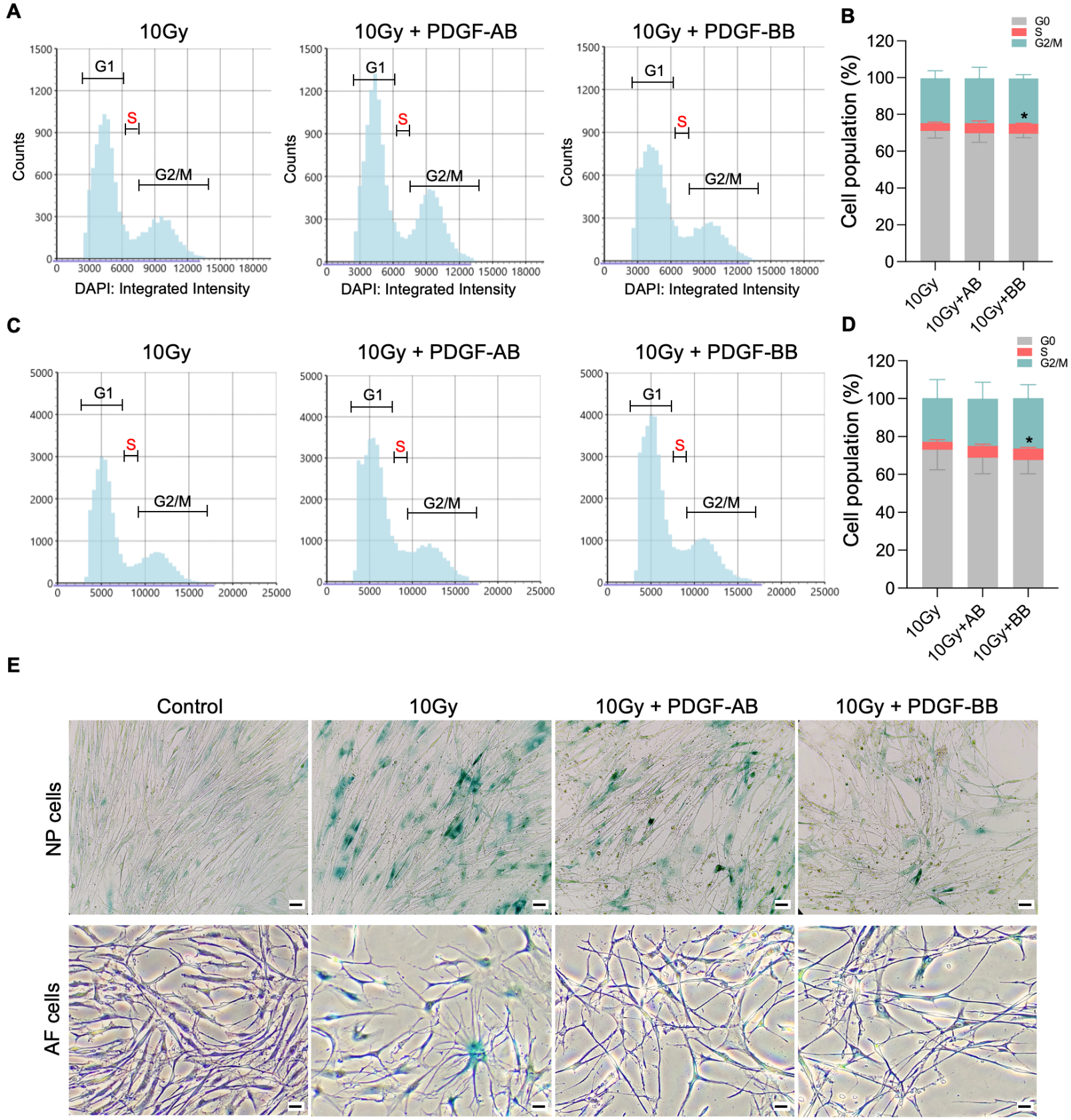
A
10Gy
10Gy + PDGF-AB
10Gy + PDGF-BB
G1
S
G2/M
Counts
DAPI: Integrated Intensity
B
G0
S
G2/M
Cell population (%)
10Gy
10Gy+AB
10Gy+BB
C
D
E
Control
NP cells
AF cells

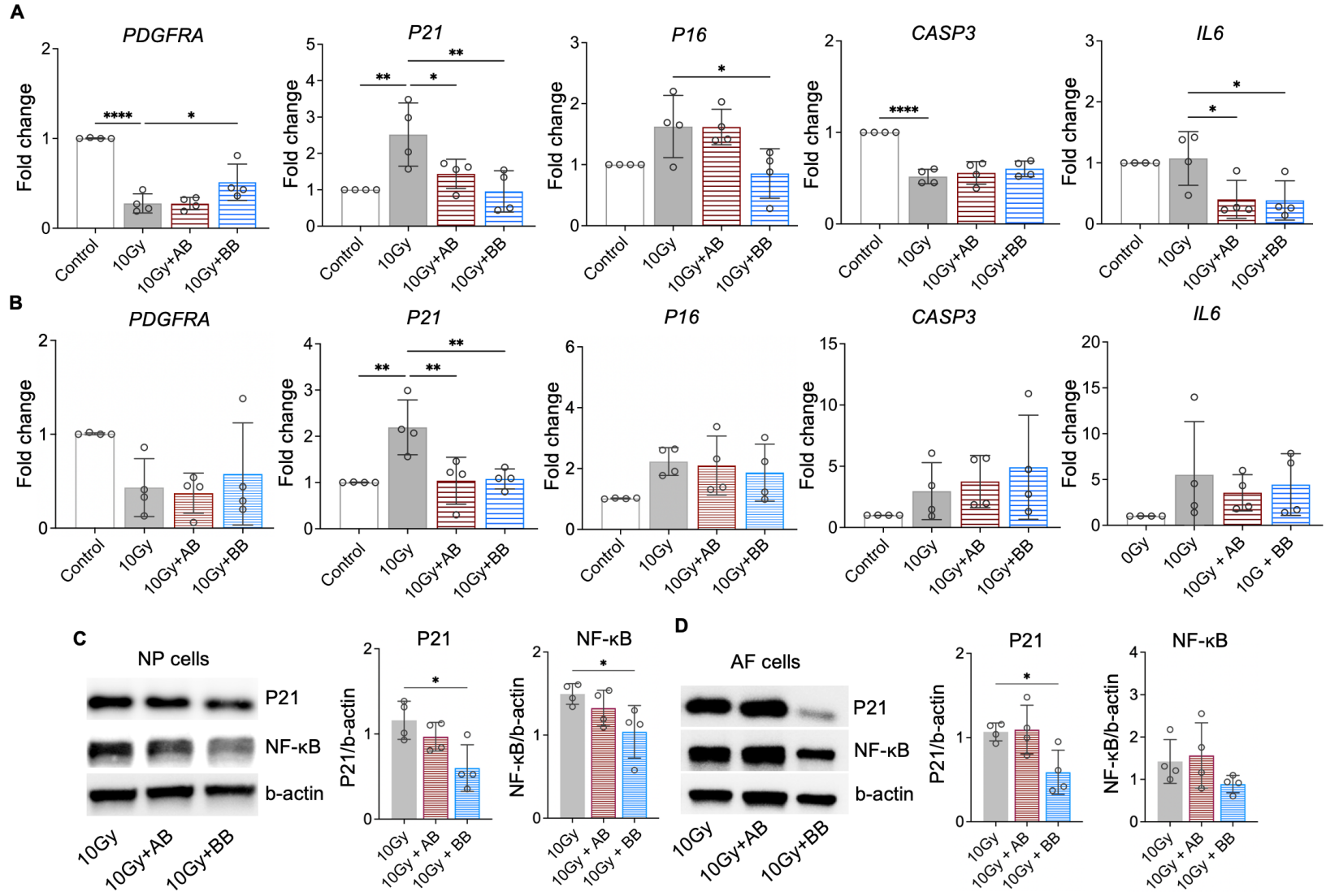
A
PDGFRA
P21
P16
CASP3
IL6
Fold change
Control
10Gy
10Gy+AB
10Gy+BB
B
PDGFRA
P21
P16
CASP3
IL6
Fold change
Control
10Gy
10Gy+AB
10Gy+BB
0Gy
10Gy + AB
10G + BB
C
NP cells
P21
NF-κB
b-actin
10Gy
10Gy+AB
10Gy+BB
P21
P21/b-actin
NF-κB
NF-κB/b-actin
10Gy
10Gy + AB
10Gy + BB
D
AF cells
P21
NF-κB
b-actin
10Gy
10Gy+AB
10Gy+BB
P21
P21/b-actin
NF-κB
NF-κB/b-actin
10Gy
10Gy + AB
10Gy + BB

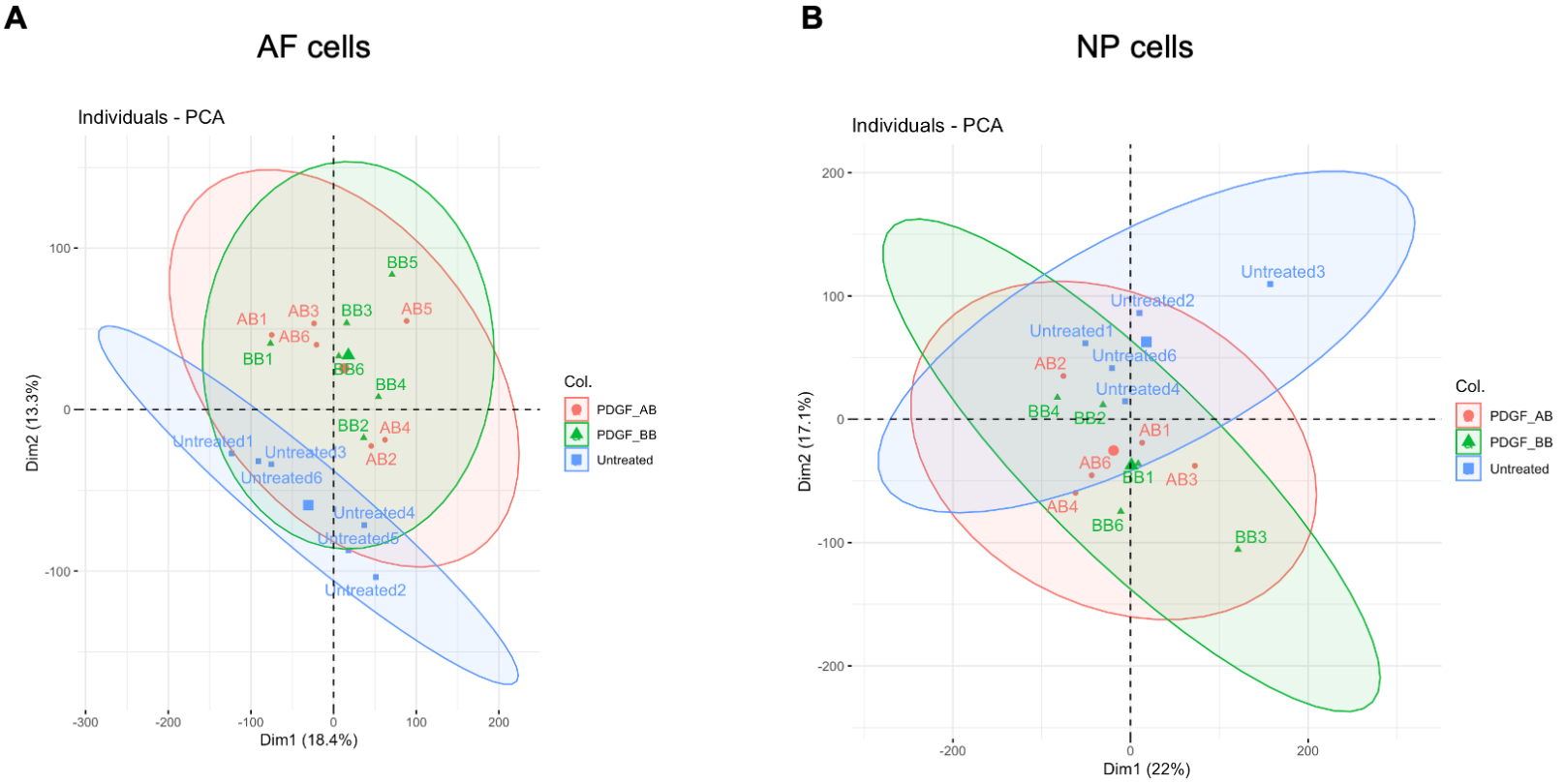
A
AF cells
Individuals - PCA
Dim1 (18.4%)
Dim2 (13.3%)
Col.
PDGF_AB
PDGF_BB
Untreated
B
NP cells
Individuals - PCA
Dim1 (22%)
Dim2 (17.1%)
Col.
PDGF_AB
PDGF_BB
Untreated